energies

MDPI

Article

Research on Application Characteristics of Zirconia-Based High-Temperature NOx Sensors

Jie Wang [1], Xi Li [2,3,*], Zhen Wang [2], Jiangtao Feng [1], Weixun Lin [2] and Jingxuan Peng [2]

[1] Changzhou Lambda Electronic Co., Ltd., Changzhou 213161, China; jason@lambdasensor.cn (J.W.); peterphon@lambdasensor.cn (J.F.)
[2] School of Artificial Intelligence and Automation, Huazhong University of Science and Technology, Wuhan 430074, China; d202080869@hust.edu.cn (Z.W.); M201972558@hust.edu.cn (W.L.); pjx@hust.edu.cn (J.P.)
[3] Technology Research Institute, Shenzhen Huazhong University of Science, Shenzhen 518055, China
* Correspondence: lixi@hust.edu.cn

Abstract: The zirconia solid electrolyte SOFC (solid oxide fuel cell) has the characteristics of oxygen ion conduction function, high-temperature resistance, thermoelectric coupling effect, etc. A NOx sensor based on zirconia solid electrolyte has common characteristics and problems with the SOFC in principle and application. The research objective of this paper is to solve the application problems of smart NOx sensors in diesel vehicles or gasoline vehicles. Improvements in the application performance of the NOx sensor can help the NOx emissions of gasoline vehicles or diesel vehicles better meet the requirements of emission regulations. The smart NOx sensor is a regulatory sensor required by vehicles for China's Phase VI Vehicle Exhaust Emission Regulations or Euro Phase VI Vehicle Exhaust Emission Regulations. The smart NOx sensor is a key sensor device for improving fuel efficiency and reducing pollution. Moreover, its measurement performance includes dynamic immunity to interference, response speed, and measurement accuracy, which are key factors affecting vehicle emissions. This paper focuses on the impact of the physical structure, electrode characteristics, and control strategies of the sensor on its performance during the application. An excellent sensor structure, electrode structure, and control strategy are given based on application analysis and experimental testing. The results show that the application performance of this smart NOx sensor meets the requirements of exhaust aftertreatment systems.

Keywords: SOFC; exhaust gas; NOx sensor; vehicle test; NOx measurement accuracy; response speed; electrode activity

Citation: Wang, J.; Li, X.; Wang, Z.; Feng, J.; Lin, W.; Peng, J. Research on Application Characteristics of Zirconia-Based High-Temperature NOx Sensors. *Energies* **2022**, *15*, 2919. https://doi.org/10.3390/en15082919

Academic Editors: Vladislav A. Sadykov and Antonino S. Aricò

Received: 19 February 2022
Accepted: 13 April 2022
Published: 15 April 2022

1. Introduction

Fossil fuel combustion is still the main energy conversion and utilization mode in China, which has low conversion efficiency and serious emission pollution. In order to achieve energy conservation and environmental protection, it is necessary to transform to a clean, low-carbon, safe, and efficient energy structure and improve the efficiency of energy conversion. At same time, it is necessary to reduce the environmental pollution caused by various products such as CO, CO_2, and NO in the combustion process. SOFCs have the advantages of high energy efficiency and low emissions because they can directly convert chemical energy from fossil fuels, biomass fuels, or other hydrocarbon fuels into electrical energy [1,2]. The core principle is the use of a special battery induction principle. The solid zirconia has the characteristics of oxygen ion conduction at high temperatures of 600~800 °C [3]. When the oxygen concentration at the electrodes on both sides of the solid electrolyte layer is different, the oxygen is catalytically ionized. A redox reaction occurs on the electrode surface [4]. At the same time, when a certain strength of voltage is applied to both ends of the electrode, the oxygen ion penetration process occurs in the electrolyte layer. Then, a stable current signal is formed on the external circuit. This process presents

an electrolytic cell effect. SOFC power generation is based on the electrical characteristics of solid zirconia matrix cells [5]. A physical diffusion barrier layer or diffusion gap is set on the gas diffusion direction, which can effectively limit the diffusion speed of the gas. Thus, the oxygen at both ends of the solid electrolyte electrode is limited, and the oxygen ion rate formed by the catalysis is limited. Finally, the current formed in the external electrical loop reaches the limit saturation state. Zirconia solid electrolyte is the material basis for SOFC and NOx sensors, and the core principles of both are the same [6,7].

With the continuous escalation of vehicle exhaust emission standards, the internal combustion engine industry has been unable to meet the requirements of energy saving and emission reduction at the same time. In order to save energy, it is necessary to improve fuel utilization, but the nitrogen oxide is generated under high temperature and oxygen-enriched conditions [8,9]. A higher-accuracy NOx and oxygen measurement is required to meet control and OBD requirements for SCR (selective catalytic reduction) systems of the diesel aftertreatment system [10–12]. Currently, people pay more attention to the pollution of NOx to the environment and the harm of NOx to human health. The NOx concentration detection and emission control technology has become the most advanced and popular research field in the world.

In terms of materials, NOx sensors are mainly divided into two categories: zirconia-based solid electrolyte and metal oxide semiconductor. Metal oxide semiconductor materials are not suitable for on-board complex environment application, due to poor stability and short service life. At present, the only mature and commercialized vehicle NOx sensor is a current type based on the limit current working principle of zirconia solid electrolyte material. This NOx sensor relies on three pumping cells, which can measure not only the NOx concentration but also the air–fuel ratio in the exhaust gas. The core ceramic element of the sensor is prepared by tape casting, screen printing, and high-temperature sintering to form a zirconia solid electrolyte [13]. The NOx sensor structure consists of three measuring chambers and three oxygen pumping cells. The three pumping cells are, respectively, composed of electrodes with two kinds of materials, which are Pt-Au and Pt-Rh alloys. Au is insensitive to NOx, and a Pt-Au alloy electrode is used to pump excess oxygen out of the chamber, but does not affect the decomposition of NOx. Rh has strong reducibility, which is very sensitive to NOx; thus, the Pt-Rh alloy electrode can be used to catalyze the reduction of NOx [13,14]. The decomposed oxygen is pumped out by the corresponding pumping cell; thus, the oxygen concentration can be detected. In applications, NOx sensor ceramic elements need to be matched with an external control and detection circuits to achieve measurement functions. The NOx working process is shown in Figure 1.

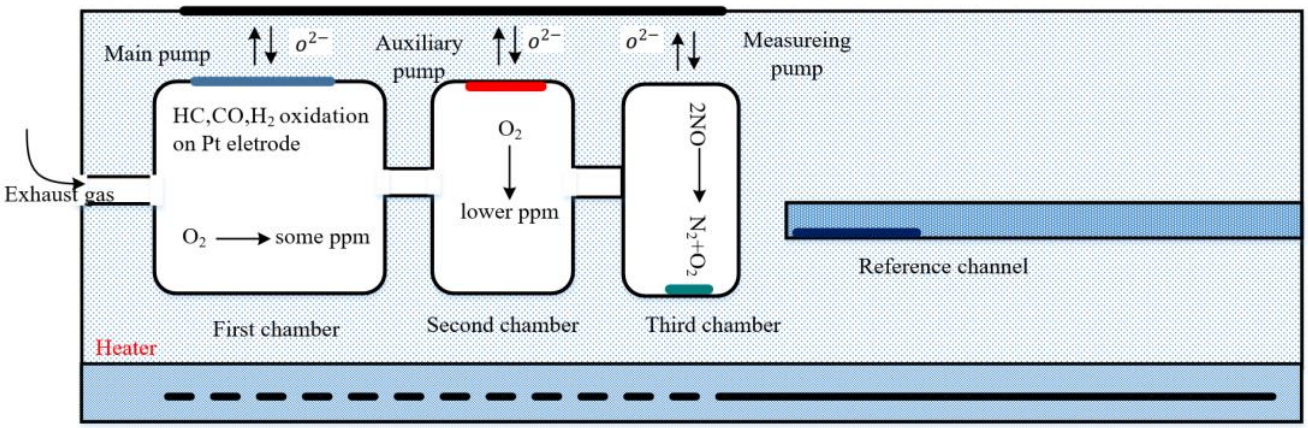

Figure 1. The diagram of NOx sensor working process.

The key performance requirements of the NOx sensor include cold start speed, dynamic response speed, and anti-interference ability, which all need to be considered when the NOx sensor is applied on vehicles [12]. However, there is a strong coupling effect between the physical structure of the three chambers, and there is also a strong coupling effect

between the three oxygen pumping cells. Thus, the closed-loop control performance of the three oxygen pumping cells is the key to the performance of the above three aspects [15]. In the research of NOx sensors, most of the current research work focuses on structural design, material application, and the electrode electrochemical mechanism model, such as electrode materials [16–18], electrolyte properties [15,19–22], cell voltages [23,24], and mechanism models [19,25–29].

Auckenthaler et al. studied the adsorption, dissociation, and mutual reaction of each gas component on the electrode surface, and then established an oxygen sensor model based on the particle occupancy of the gas adhesion points on the electrode surface [30]. Mitterdorfer et al. studied in-depth the adsorption of gaseous oxygen molecules on the metal electrode surface, the diffusion of adsorbed atomic oxygen on the electrode surface, and the charge transfer reaction of atomic oxygen at the three-phase interface. Furthermore, they constructed the micro-kinetic model of the electrode and electrolyte system [31]. The research of Velle et al. and Okamotoa et al. showed that when the temperature T > 800 °C, the whole reaction was controlled by charge transfer. It was found that the diffusion of atomic oxygen on the electrode surface was considered to be the reaction rate-determining step when 600 °C < T < 750 °C. However, it is believed that the dissociative adsorption of oxygen molecules on the metal electrode dominates while T < 500 °C [32,33]. The activities of Pt-YSZ, Pt-Au-YSZ, and Rh-Pt-Au-YSZ thick-film electrodes in O_2, N_2 and NO, N_2 gas mixtures at high temperatures were investigated by electrochemical impedance spectroscopy (EIS) and linear sweep voltammetry (LSV) by Schmidt-Zhang et al., and the experiments results indicated that the Rh-Pt-Au mixture is a suitable working electrode material for amperometric NOx sensors based on the solid electrolyte (YSZ) [16]. Tadashi et al. studied NOx in the decomposition mechanism on the Pt and Pt-Au electrodes, and the conclusion was reached that an increase in the activation energy for NO dissociation enables the preferential oxygen pumping on the Pt-Au electrode [19]. Brailsford et al. studied the physical and chemical processes involved in the working process of the sensor in detail. A first-principles model of the zirconia oxygen sensor was also established [15]. Yusuke et al. designed a new NOx sensor to achieve high accuracy and a quick light-off time with an additional electrode placed next to the NOx detection electrode to eliminate the impact of residual O_2 and conducted electrons [2]. Hisashi et al. developed a higher-accuracy NOx sensor by optimizing the sensing element temperature control and reducing the leakage current to the NOx pumping electrode [12].

None of the above studies have in-depth analysis and research on the dynamic application of NOx sensors under different engine load conditions in vehicles. For example, during acceleration transients, the oxygen concentration in the exhaust gas changes sharply, which interferes with the NOx sensor steady-state measurements and results in a decrease in response speed and measurement accuracy. At the same time, it is important to improve the accuracy of NOx measurement under the conditions of backduging and extreme working conditions, in which the oxygen concentration is less than 0%.

In our previous research work, a comprehensive electrochemical model including concentration overpotential, activation overpotential, and ohmic overpotential was developed for the main oxygen pumping cell of the sensor. A diffusion model was also developed to describe the change in gas concentration. Then, the electrochemical model and the diffusion model were combined through the limit current. One important feature of this combined model is that the model eliminates the intermediate variable (gas concentration) and only shows the relationship between the pumping voltage and the pumping current. In order to validate the model at different gas concentrations, the model results were compared with experimental measurements obtained on a designed sensor test rig. Furthermore, the overpotentials of the cathode and the anode were compared to determine the dominant electrode. The changes in the internal characteristics of the sensor during operation were analyzed, which will provide guidance for the design and control of the sensor [29]. In this paper, the dynamic problems of NOx sensors in the application of the aftertreatment system for China's phase VI emission regulations are studied. In addition, combining the structure

of the sensor and the characteristics of electrode materials, the control process parameters and control algorithms are studied to improve the dynamic measurement accuracy and response speed of NOx on vehicle applications.

2. The Working Principle

As shown in Figure 2, the NOx sensor structure consists of three chambers, three pumping cells, a heater, and five signal electrodes [2]. Figure 3 shows a control logic block diagram. At the working state, the zirconia element is heated to around 780 °C. When the exhaust gas enters the first chamber, the CO, H_2, and unburned hydrocarbon in the exhaust gas are oxidized. Moreover, some of the NO is oxidized to NO_2. In addition, the oxygen in the first chamber is pumped out by the first pumping cell with the application of pump voltage Vp_0, so the oxygen concentration in the first chamber is controlled to a low ppm value. Then, the exhaust gas further diffuses into the second chamber, in which the oxygen is pumped out further by the second pumping cell with the application of voltage Vp_1. The oxygen concentration in the second chamber reaches a very low value without NO to decompose. Finally, the NO in the exhaust gas further diffuses into the third measuring chamber, where the NO is catalytically decomposed by the Rh-Pt electrode to form N_2 and O_2. The limit pumping current Ip_2 of oxygen is formed when the oxygen decomposed from NO is pumped out through the measuring pumping cell, which has a linear relationship with NO. All three oxygen pumping cells have the function of pumping oxygen in both directions [34–36]. The Table 1 is the definition of the structure symbol of the ceramic element.

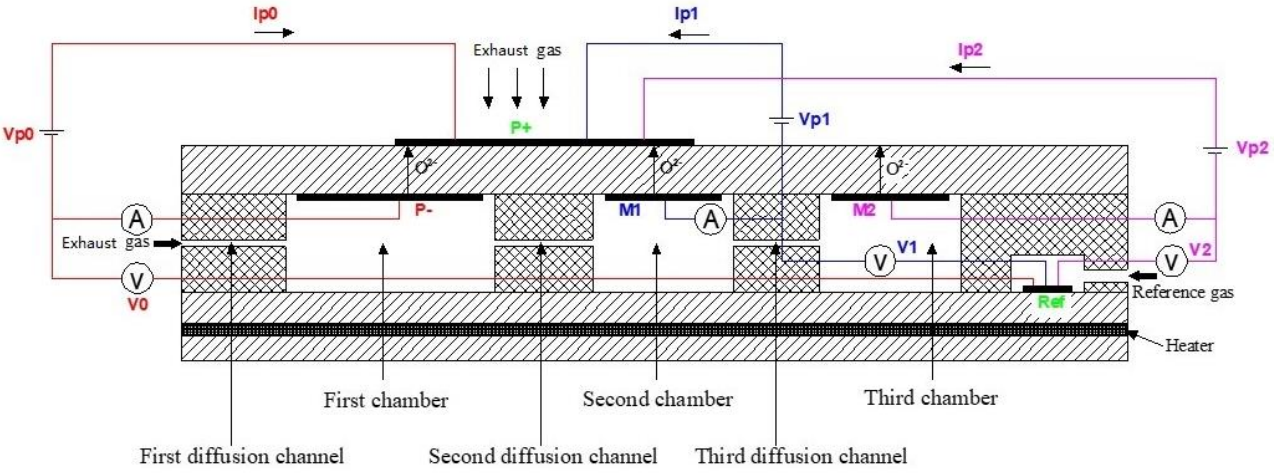

Figure 2. The structure block diagram of NOx sensor ceramic element.

The NOx sensor ceramic element is assembled in structural parts to meet the application requirements such as heat dissipation, insulation, sealing, waterproofing, and diversion. The NOx sensor ceramic element needs to match the external drive control to achieve the detection and output of NOx concentration. The external circuit consists of feedback heating control based on a three-wire heater or internal resistance, closed-loop control of pumping cells, and pumping current detection circuits. Three closed control loops of pumping cells are coupled to each other because the chambers and diffusion gaps are structurally coupled. The three pump oxygen cells have the Ip_1, V_1, and V_2 set points, which are the inputs of the control target variables, while the control variables are Vp_0, Vp_1, and Vp_2. The set points of Ip_1, V_1, and V_2 affect the response speed and accuracy of NOx dynamic and static measurements. The Ip_1 set point indicates the diffusion flow of the oxygen from the first chamber to the second chamber, and the value of Ip_1 is associated with the oxygen concentration of the first chamber. The set point of V_1 determines the oxygen concentration in the second chamber under steady-state conditions, which also affects the decomposition state of the NO_2 in the second chamber. The V_2 set point must be

greater than the set point of V_1 to ensure that oxygen does not diffuse in reverse, and the set point of V_2 needs to ensure that the measuring pump reaches the limit state to promote NO decomposition on the measuring electrode.

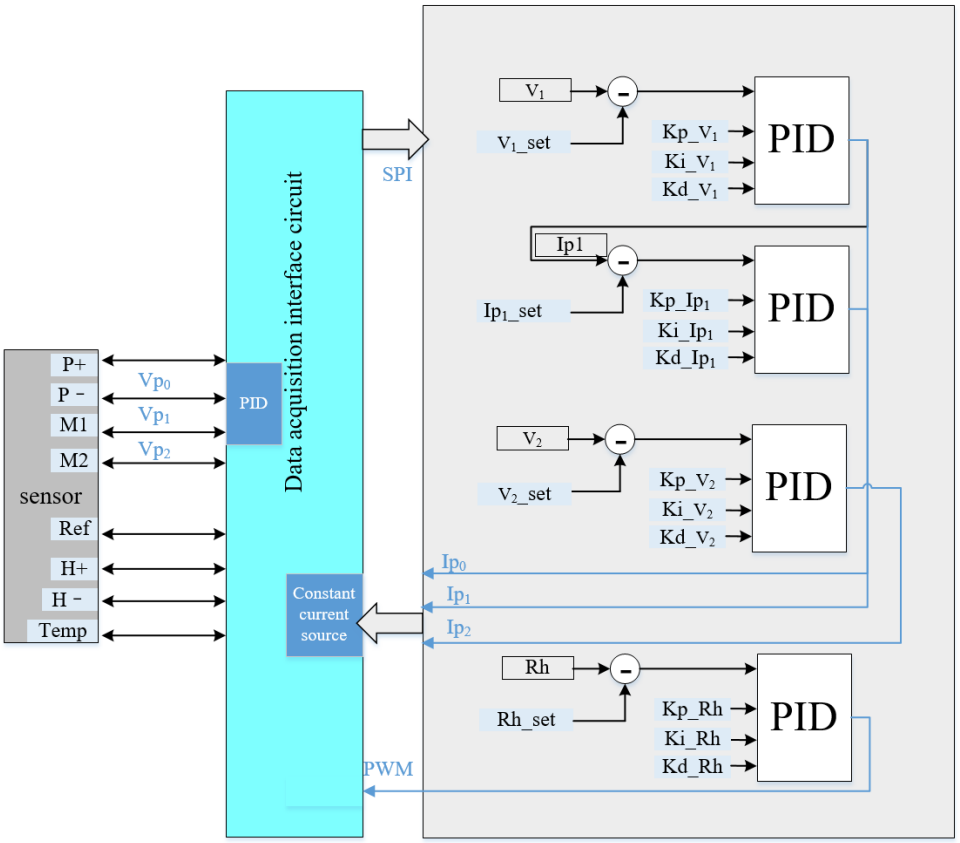

Figure 3. NOx sensor control logic diagram.

Table 1. Symbol description.

Symbol	Description
P+	Common external electrode of pump cell
P−	Internal electrode of main pump cell
M1	Internal electrode of auxiliary pump cell
M2	Internal electrode of measuring pump cell
Ref	reference electrode
Ip_0	Pumping current of main pump cell
Ip_1	Pumping current of auxiliary pump cell
Ip_2	Pumping current of measuring pump cell
C0, C1, C2	Three chambers
Vp_0	Pumping voltage of main pump cell between P+ and P−
Vp_1	Pumping voltage of auxiliary pump cell between P+ and M1
Vp_2	Pumping voltage of measuring pump cell between P+ and M2
V_0	Nernst voltage in the first chamber between Ref and P−
V_1	Nernst voltage in the second chamber between Ref and M1
V_2	Nernst voltage in the third chamber between Ref and M2
D0, D1, D2	Three diffusion channels

3. Problem Description in Vehicle Application

To meet China's Phase VI Vehicle Exhaust Emission Regulation, the exhaust gas aftertreatment system needs to install two NOx sensors, namely the pre-NOx sensor and after NOx sensor. As shown in Figure 4, the pre-NOx sensor is installed at the EGR inlet or DPF outlet, while the after-NOx sensor is installed at the outlet of the entire exhaust gas

aftertreatment system [2]. Because they are installed in different locations, the functions of these two sensors are also different. The output of the pre-NOx sensor is used as a key input parameter for the execution of the urea injection strategy. The output of the after-NOx sensor is used for real-time monitoring of exhaust emissions and OBD diagnostics. The atmosphere at the installation location of the pre-NOx sensor is very complicated, and the oxygen concentration changes drastically. When the DPF is regenerated or the acceleration displacement changes sharply, there is a large disturbance of Ip_2 current output, which makes the closed-loop control of the pumping cell out of the stable range in the transient process. The magnitude of the interference depends on the severity of the change in oxygen concentration, as shown in Figure 5. On the one hand, the oxygen concentration first increases and then decreases, which results in an increase in the oxygen concentration in the first chamber when the throttle opening increases. Then, the pumping current Ip_1 and the Nernst voltages V_1 and V_2 are out of the stable range with the change in oxygen concentration in the second and third chambers, which result in fluctuations in pumping current Ip_2 corresponding to NOx concentration. Large deviations in NOx measurement affect the accuracy of the urea injection and result in the exhaust emission that does not meet the regulatory requirements. On the other hand, excessive fuel injection leads to insufficient combustion, producing NOx and reducing substances. When the exhaust gas enters the first chamber, those reducing and oxidizing substances react on the catalytic electrodes, resulting in a NOx concentration measurement value lower than the actual value. However, the reduction reaction of NOx under this operating condition can be effectively suppressed when the oxygen concentration is high in the first chamber. In the pump control loop, the value of Ip_1 can be set to a larger value, which means that the oxygen concentration in the first chamber is high. It is also found that the set points of Ip_1, V_1, and V_2 have great impact on the amplitude of transient interference. Therefore, it is necessary to study the influence of the steady-state set points of Ip_1, V_1, and V_2 on the dynamic response speed and measurement accuracy.

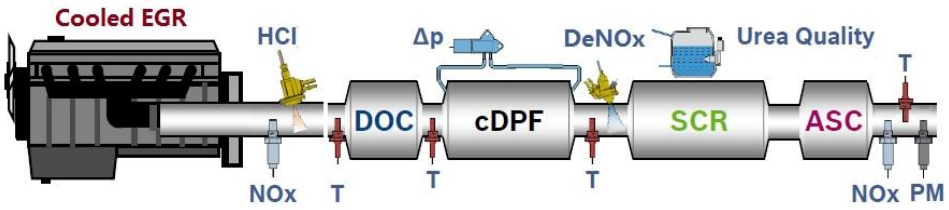

Figure 4. Diesel exhaust aftertreatment system.

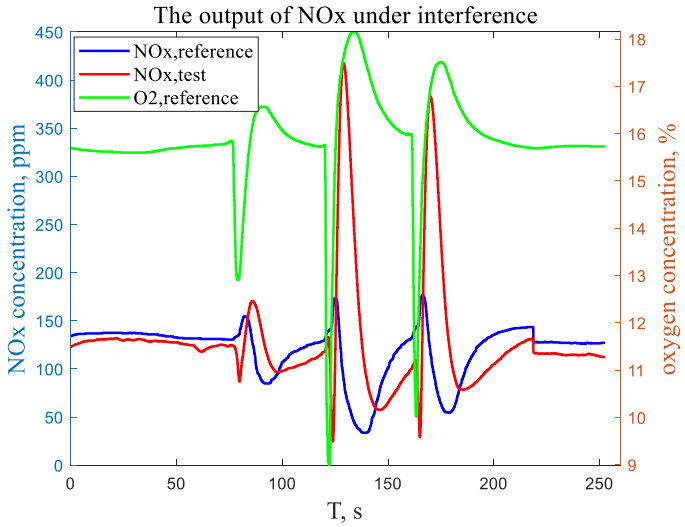

Figure 5. The output of NOx under interference.

4. Theoretical Analysis and Experiments

4.1. Theoretical Analysis

In a steady state, it is assumed that the oxygen concentration of exhaust gas is $c_{O_2,env}$, the first chamber oxygen concentration is $c_{O_2,fc}$, and the second chamber oxygen concentration is $c_{O_2,sc}$. The relationship between the pumping voltages Vp_0, Vp_1 and Nernst voltages V_0, V_1 is as follows.

$$Vp_0 = E_p^0 + \frac{RT_{cell}}{nF} \ln \frac{P_{O_2,env}}{P_{O_2,fc}} + \eta_1, V_{P+,P-} \tag{1}$$

$$V_0 = E_N^0 + \frac{RT_{cell}}{nF} \ln \frac{P_{O_2,ref}}{P_{O_2,fc}}, V_{Ref,P-} \tag{2}$$

$$Vp_0 = V_0 + \frac{RT_{cell}}{nF} \ln \frac{P_{O_2,env}}{P_{O_2,ref}} + \eta_1, V_{P+,P-} \tag{3}$$

$$\Delta V = Vp_0 - V_0 = \frac{RT_{cell}}{nF} In\left(\frac{P_{env}}{P_{ref}}\right) + \eta_1 \tag{4}$$

$$Vp_1 = E_{p1}^0 + \frac{RT_{cell}}{nF} \ln \frac{c_{O_2,env}}{c_{O_2,sc}} + \eta_2, V_{P+,M1} \tag{5}$$

$$V_1 = E_{n1}^0 + \frac{RT_{cell}}{nF} \ln \frac{c_{O_2,ref}}{c_{O_2,sc}}, V_{Ref,M1} \tag{6}$$

$$Vp_1 = V_1 + \frac{RT_{cell}}{nF} \ln \frac{P_{O_2,env}}{P_{O_2,ref}} + \eta_1, V_{P+,M1} \tag{7}$$

where $P_{O_2,env}$ represents the oxygen partial pressure of the exhaust gas; $P_{O_2,fc}$, $P_{O_2,sc}$, P_{ref}, respectively, represent the oxygen partial pressure of the first, second, and reference chambers, and η_1, η_2 represent the overpotential of the electrode.

The relationship between the oxygen diffusion flow and the oxygen partial pressure in the chambers is as follows.

$$\mathrm{N} = \frac{D_1 S_1}{RTL_1}\left(P_{O_2,env} - P_{O_2,fc}\right) \tag{8}$$

$$\mathrm{N}_2 = \frac{D_2 S_2}{RTL_2}\left(P_{O_2,fc} - P_{O_2,sc}\right) \tag{9}$$

$$\mathrm{N}_1 = \mathrm{N} - \mathrm{N}_2 \tag{10}$$

where N represents the flow of oxygen diffused into the first chamber, N_1 represents the oxygen flow pumped out from the first chamber, and N_2 represents the oxygen diffused into the second chamber.

According on the relationship between the pumping current and the oxygen flow, there is

$$\begin{aligned} Ip_0 = 4F\mathrm{N}_1 = & \frac{4FD_1S_1\left(P_{O_2,env}-P_{O_2,fc}\right)}{RT_{cell}L_1} - \frac{4FD_2S_2\left(P_{O_2,fc}-P_{O_2,sc}\right)}{RT_{cell}L_2} \\ & = \frac{4FD_1S_1\left(P_{O_2,env}-P_{O_2,fc}\right)}{RT_{cell}L_1} - Ip_1 \end{aligned} \tag{11}$$

$$Ip_1 = 4F\mathrm{N}_2 = \frac{4FD_2S_2\left(P_{O_2,fc} - P_{O_2,sc}\right)}{RT_{cell}L_2} \tag{12}$$

The relationship between concentration and pressure is known as $= \frac{P}{RT}$; therefore

$$Ip_0 = \frac{4FD_1S_1\left(c_{O_2,env} - c_{O_2,fc}\right)}{L_1} - Ip_1 \tag{13}$$

$$c_{O_2,fc} = c_{O_2,env} - \frac{L_1(Ip_0 + Ip_1)}{4FD_1S_1} \tag{14}$$

$$Ip_1 = \frac{4FD_2S_2\left(c_{O_2,fc} - c_{O_2,sc}\right)}{L_2} \tag{15}$$

Then,

$$P_{O_2,fc} = P_{O_2,ref}e^{(E_N^0 - V_0)\frac{nF}{RT_{cell}}} \tag{16}$$

$$c_{O_2,fc} = P_{O_2,fc}/RT_{cell} \tag{17}$$

$$P_{O_2,env} - \frac{L_1(Ip_0 + Ip_1)}{4FD_1S_1} * RT_{cell} = P_{O_2,ref}e^{(E_N^0 - V_0)\frac{nF}{RT_{cell}}} \tag{18}$$

$$P_{O_2,env} - \frac{L_1(Ip_0 + Ip_1)}{4FD_1S_1} * RT_{cell} = P_{O_2,ref} * e^{E_N^0} * e^{-V_0 * P_{O_2,ref} * \frac{nF}{RT_{cell}}} \tag{19}$$

It is found that the value of Ip_1 is exponentially related to V_0 under steady-state conditions when the external oxygen concentration $c_{O_2,env}$ remains unchanged and Ip_0 remains unchanged in the limiting current state.

It is found that Vp_0 and V_0 show a linear relationship from Formula (3) when the external oxygen concentration $c_{O_2,env}$ remains unchanged.

It is found that Vp_0 and Ip_1 show a logarithmic relationship from Formulas (3), (18) and (19) when the external oxygen concentration $c_{O_2,env}$ remains unchanged.

4.2. Test Equipment and Test Methods in Laboratory

The test equipment included NOx synthetic gas equipment, a propane burner stand apparatus, and a diesel pickup truck, as shown in Figures 6–8. In the NOx synthetic gas equipment, the N_2, O_2, NO, and gas mixture (H_2, CO, CO_2 in N_2) can be allocated to simulate the changes in oxygen concentration and NOx concentration. The static output characteristics of the NOx sensor were studied on the NOx synthetic gas equipment. A propane burner stand apparatus was used to simulate the gasoline combustion process with propane. Some NO could be added to the exhaust gas. The influence of the oxygen concentration in the first chamber and the activity of the measuring electrode in the first chamber on the measurement accuracy of the NOx sensor were studied on the propane burner stand apparatus. In addition, the driving dynamic characteristics of the NOx sensor were studied on the diesel pickup truck, which had an exhaust aftertreatment system consisting of DOC, DPF, SCR, and ASC. Two NOx sensors were installed on this system. The emission of the diesel pickup truck vehicle complied with the China's phase VI vehicle emission regulations. Some application characteristics of the NOx sensor were studied and tested on the customer's engine test bench and revolving drum test bench, as shown in Figure 9.

4.3. Test Results

The NOx sensor was in normal operation, and the oxygen was set to 21% in vol. The V_0 output was recorded with the change in the Ip_1 set point in the pump closed control loop, as shown in Figure 10.

The NOx sensor was in normal operation, and the oxygen was set to 21% in vol. From Figure 11, it can be seen that the output value of V_0 increased with Vp_0, which showed a linear relationship.

As can be seen in Figure 12, the output value of Ip_1 decreased with Vp_0, which showed a logarithmic relationship when the Ip_1 and Vp_0 operated in an open-loop state.

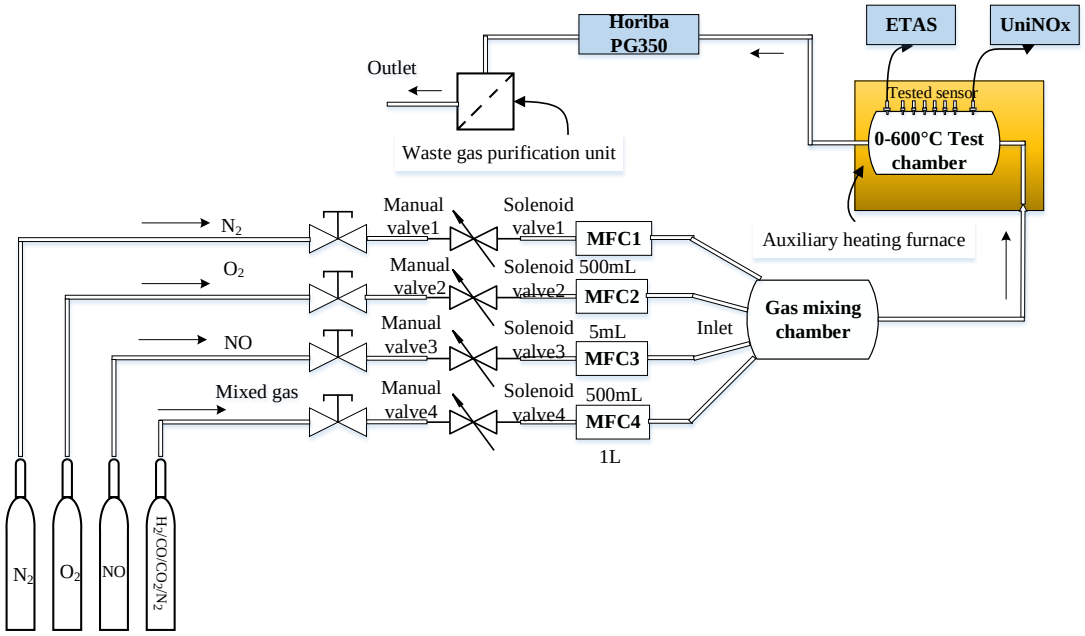

Figure 6. NOx synthetic gas equipment.

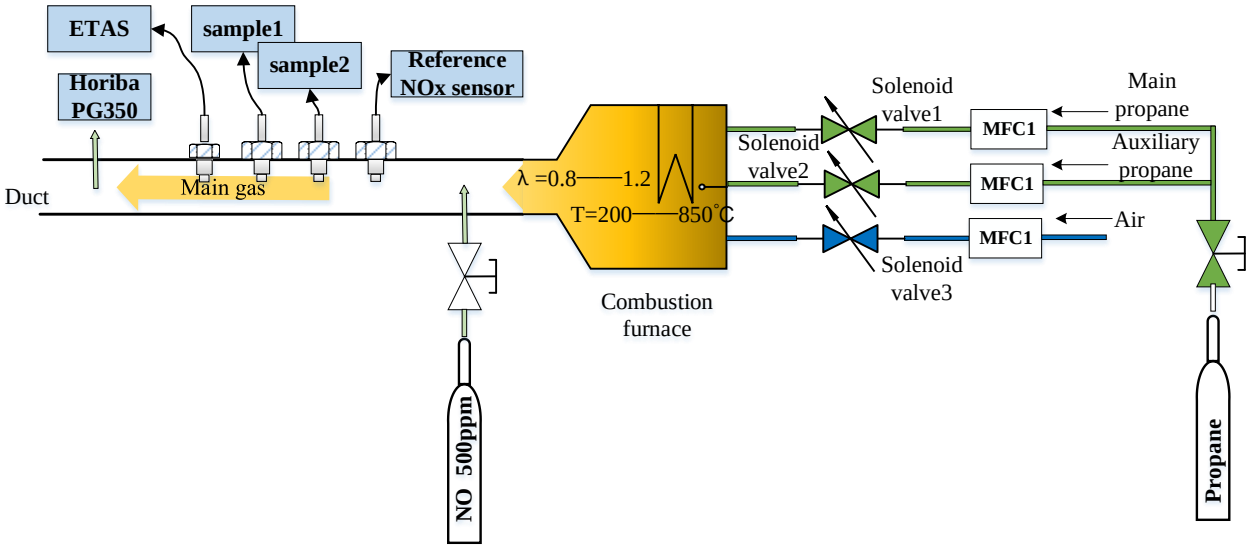

Figure 7. Propane burner stand apparatus.

Figure 8. Diesel pickup truck.

Figure 9. Revolving drum test bench.

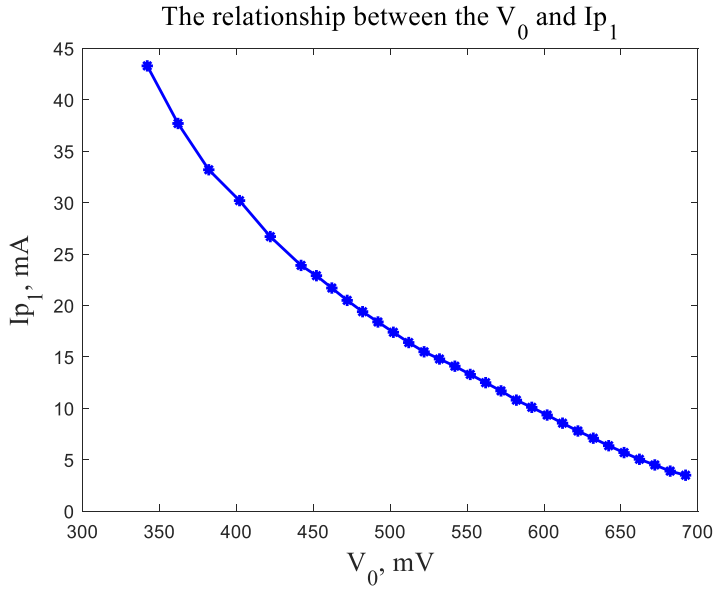

Figure 10. The relationship between the V_0 and Ip_1.

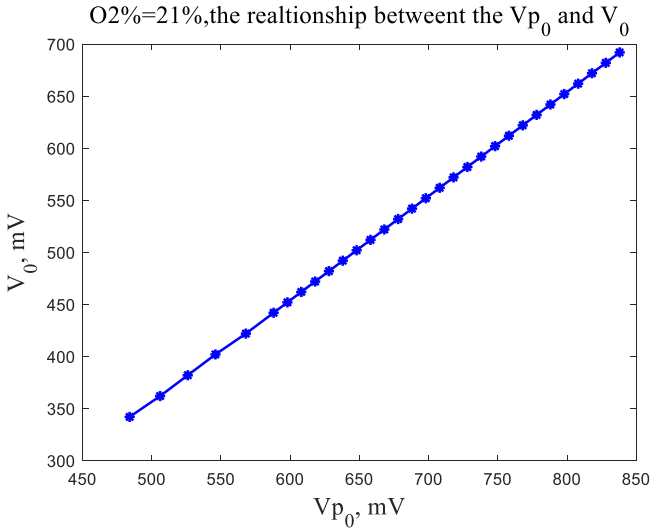

Figure 11. The relationship between the V_0 and Vp_0.

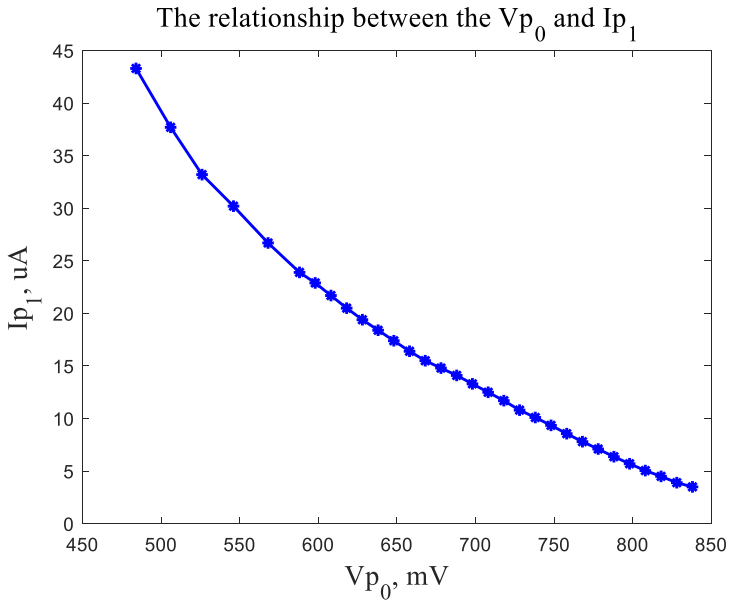

Figure 12. The relationship between the Vp_0 and Ip_1.

On the one hand, the oxygen concentration in the first chamber depended on the input setpoint of the Vp_0 and Ip_1 closed control loop. Four group tests were conducted on the diesel pickup truck with different Ip_1 set values, and the input of exhaust oxygen concentration and the outputs of V_0, Ip_1, and Ip_2 (corresponds to NOx concentration) were recorded by the data acquisition device, as shown in Figure 13. It was found that the partial pressure of the external oxygen concentration decreased when the throttle opening changed from small to large. The output steady-state value of V_0 was small and the oxygen concentration in the first chamber was in a lean state when Ip_1 was set to a larger value. Then, the output fluctuation amplitudes of Ip_1 and V_0 were relatively small when the external oxygen concentration changed by the same magnitude. Thus, the oxygen concentration of the second chamber could be quickly adjusted to a stable state, which reduced the interference with the oxygen concentration of the third chamber. In conclusion, the changes in external oxygen concentration had little interference with Ip_2 (corresponds to NOx concentration), the process of Ip_2 recovering from dynamic to steady state was smoother, and the accuracy of the NOx measurement and response speed was improved, as shown in Figure 13d.

On the other hand, the oxygen concentration in first chamber also depended on the structural characteristics and electrode characteristics when the Ip_1 set point was identical to each other among several ceramic elements. In order to maintain the oxygen concentration of the first chamber, the Ip_1 input value of the Ip_1 and Vp_0 closed control loop should be set according to the diffusion capacity of the second diffusion channel, which can be seen in Table 2. The Ip_1 set value should decrease with the diffusion capacity of the second diffusion channel. The structure diagram of the diffusion channel and the slice diagram of the ceramic element are shown in Figure 14.

At the same time, the activity of the main pump electrode P- also had influence on the oxygen concentration of the first chamber when the Ip_1 set value was the same as each other among several ceramic elements. In the measuring principle, the electrodes of the main pump electrode P− were mainly used to oxidize CO, CH, and NO to CO_2, H_2O, and NO_2. A reasonable oxygen concentration must be set in the first chamber to ensure that CO and CH are fully oxidized and NO is oxidized in small amounts or none. When the oxygen concentration in the first chamber was insufficient, NOx reacted with CO, CH, etc. so that the measured value of NOx was low.

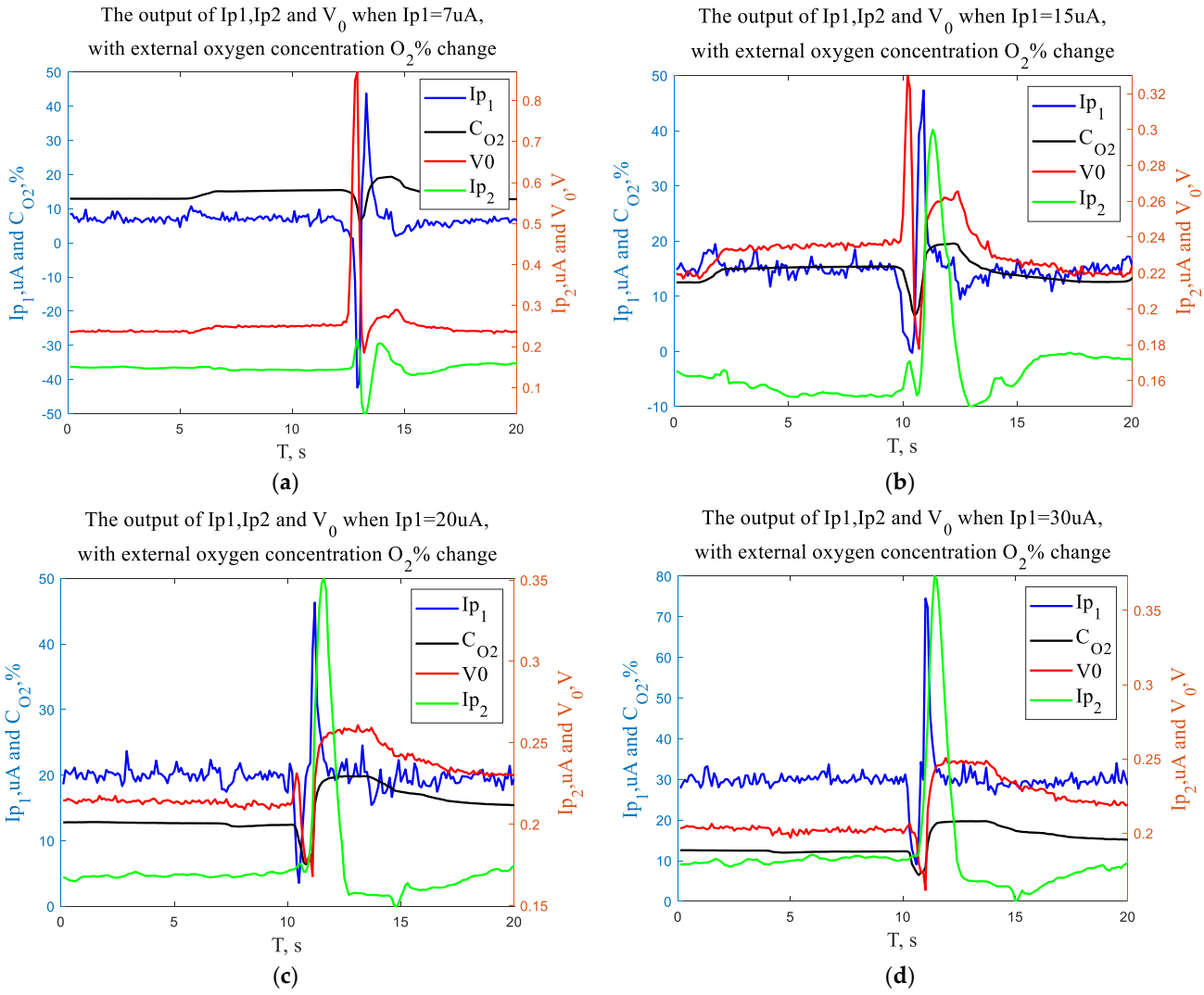

Figure 13. The outputs of Ip_1, Ip_2, and V_0 when the oxygen concentration interference amplitude was the same.

Table 2. Ip_1 set point for different structure sizes of the second diffusion channel.

Second Diffusion Channel Structure Size	Ip_1 Set Point	Ip_1 Limit Current Value in Air
D1: L = 600 μm, W = 2500 μm, H = 16 μm	35 μA	1.45 mA
D1: L = 600 μm, W = 1500 μm, H = 16 μm	25 μA	1.25 mA
D1: L = 600 μm, W = 800 μm, H = 8 μm	15 μA	1.12 mA

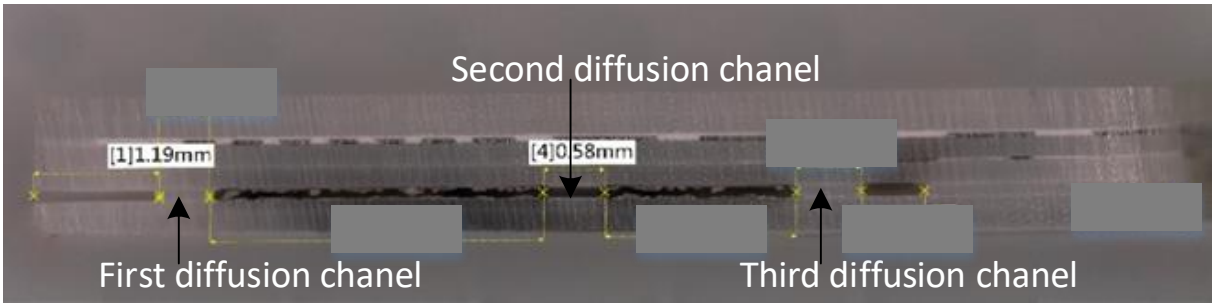

Figure 14. The slice diagram of ceramic element.

As shown in Figure 15, two NOx sensors were assembled with two ceramic elements based on two kinds of main pump electrode P−. They were installed on the pipe of the propane burner stand apparatus. The NO was added to the exhaust gas of the propane burner stand apparatus, and the concentration of NO in mixed exhaust gas could reach 500 ppm or other values when the exhaust was under a rich state. The measurement values of NOx sensors were different, and the measurement value of the NOx sensor with high activity of the main pump electrode P− was lower than that with low activity of the main pump electrode P−, as shown in Table 3.

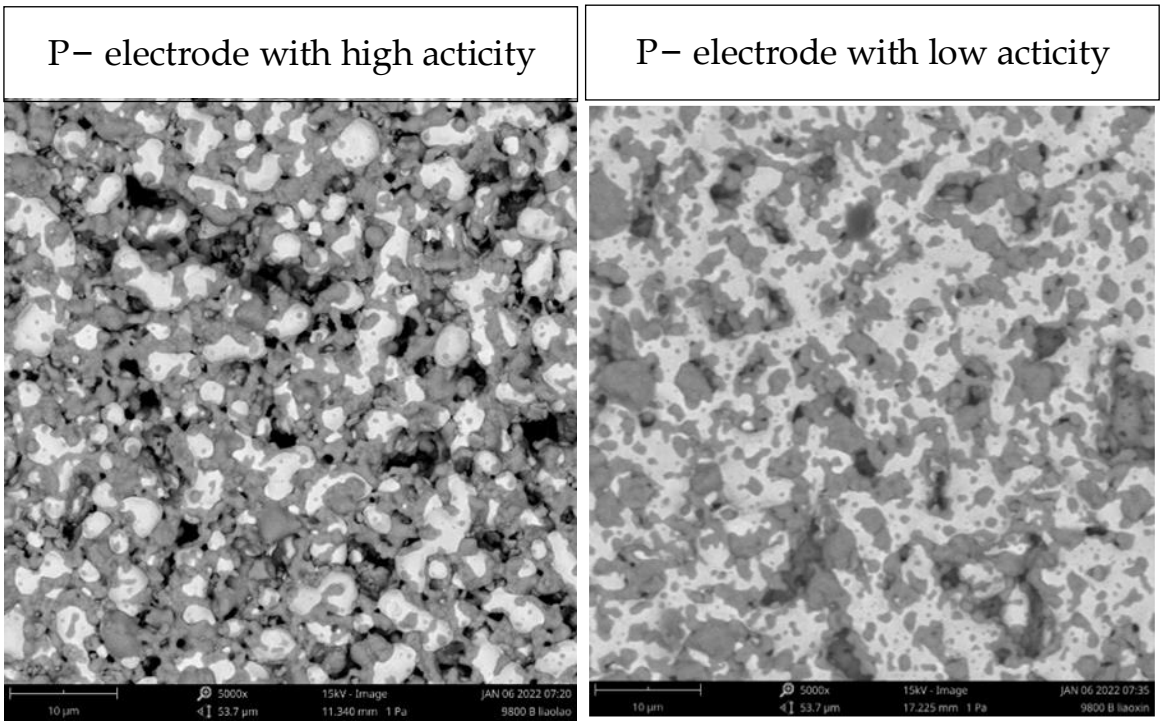

Figure 15. The structure of P− electrode with high and low activity.

Table 3. The measurement values of the NOx sensor with high- and low-activity P− electrode (sample1 has high-activity P− electrode, sample2 has low-activity P− electrode).

Num.	λ = Air Fuel Ratio/14.7	Ip_0 μA	Ip_1 μA	Ip_2 μA	O_2%	NOx ppm
Sample1	λ = 1.000	−32	20	0.772	0.18	473
Sample2		−32	20	0.778	0.19	475
Reference NOx sensor		-	-	-	0.21	501
Sample1	λ = 0.965	−186	20	0.747	−1.34	453
Sample2		−190	20	0.778	−1.35	475
Reference NOx sensor		-	-	-	−1.29	481
Sample1	λ = 0.935	−315	20	0.52	−2.51	294
Sample2		−311	20	0.721	−2.45	435
Reference NOx sensor		-	-	-	−2.44	458
Sample1	λ = 0.912	−445	20	0.324	−3.69	157
Sample2		−438	20	0.647	−3.65	383
Reference NOx sensor		-	-	-	−3.63	389
Sample1	λ = 0.890	−560	20	0.159	−4.69	58
Sample2		−558	20	0.593	−4.63	345
Reference NOx sensor		-	-	-	−4.58	353

In the application, it was also found that the NOx measurement value increased with the oxygen concentration in the first chamber when the NO concentration in the environment was fixed. The NO was excessively oxidized to NO_2 after entering the first

chamber when the oxygen concentration in the first chamber was high and the activity of pump electrode P− was high. The NO_2 diffused into the second and third chamber, and more oxygen ions formed on the measurement M2 electrode because there were two oxygen atoms in NO_2. Then, the pumping current increased with the oxygen concentration in the environment, as shown in Figure 16. Thus, it was necessary to set an appropriate activity for the pump electrode P−. In addition, the pumping current output correction algorithm should be introduced, such as the two-dimensional linear interpolation correction algorithm based on oxygen concentration and NOx concentration, as shown in Figure 17 and Table 4. The final NOx measurement value was multiplied by a correction factor. The improvement of the measurement accuracy by the correction algorithm is shown in Figure 18.

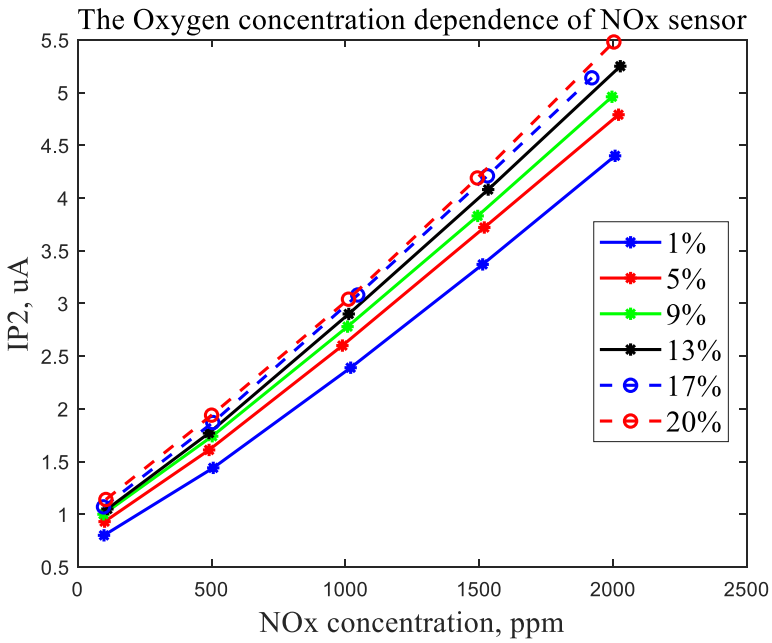

Figure 16. The oxygen concentration dependence of the NOx sensor.

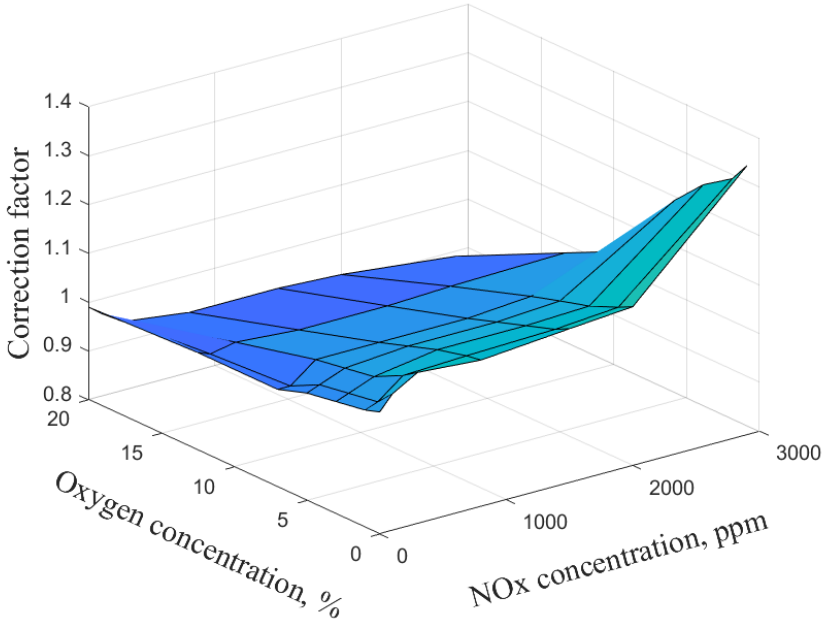

Figure 17. Two-dimensional linear interpolation correction algorithm output.

Table 4. The calibration parameters of the NOx sensor for oxygen concentration dependence.

NOx Concentration / O_2 Concentration — Correction Factor	0.00 ppm	100.00 ppm	300.00 ppm	800.00 ppm	1500.00 ppm	2000.00 ppm	2900.00 ppm
0.00%	1.05	1.08	1.11	1.10	1.12	1.13	1.35
1.00%	1.04	1.05	1.09	1.10	1.10	1.11	1.31
3.00%	1.03	1.04	1.06	1.08	1.08	1.09	1.27
5.00%	1.02	1.03	1.05	1.06	1.06	1.07	1.21
7.00%	1.00	1.00	1.04	1.04	1.04	1.05	1.08
12.50%	1.00	0.99	1.00	0.99	0.99	1.00	1.00
20.00%	0.99	0.97	0.94	0.92	0.92	0.92	0.89

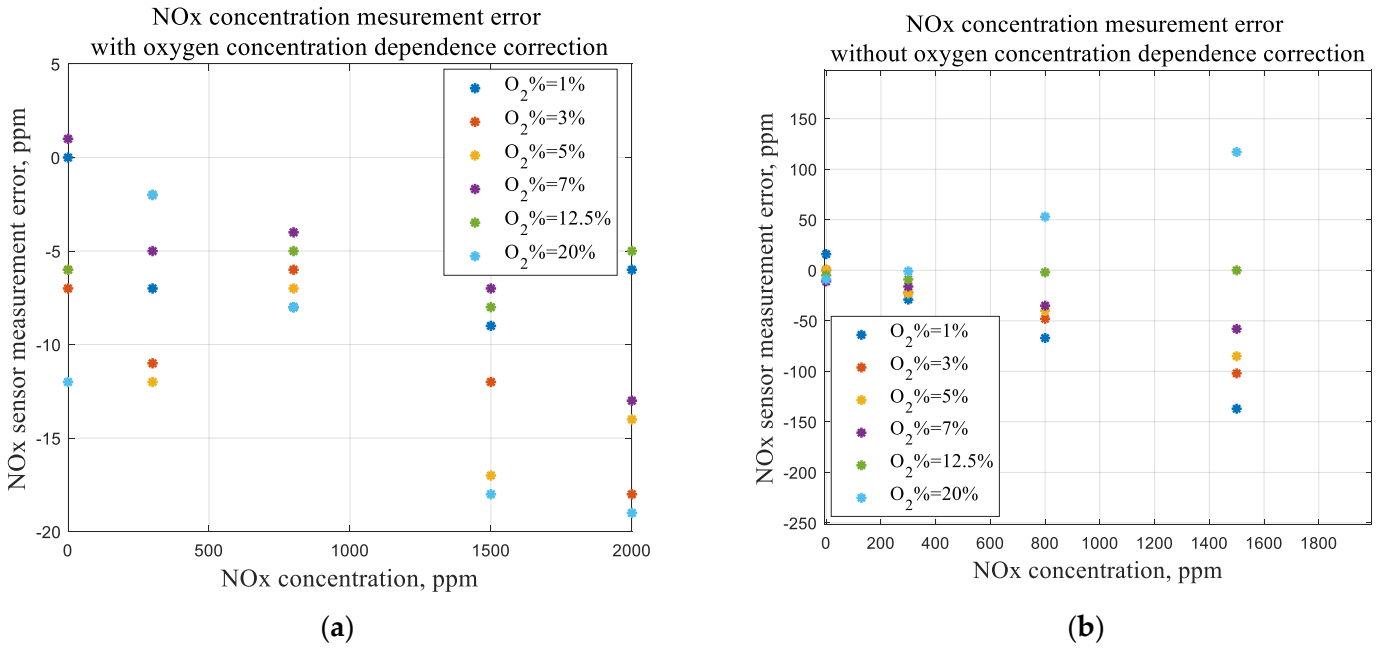

Figure 18. The calibration results for oxygen concentration dependence.

4.4. Diesel Engine Bench and Revolving Drum Test

The dynamic test was conducted on the diesel engine bench. The test results showed that the output of the NOx measurement value of the test sample was the same as that of the reference equipment when the input of Ip_1 was set as 25 μA and the activity of the measurement electrode P− was set to low; the test results are shown in Figure 19. Then, the WLTC cycle test was conducted on the revolving drum test bench. The result showed that the NOx emission can meet the GB6b standard of China, which can be seen in Figure 20 and Table 5. At the same time, the dynamic output of the test sample could track the output of the reference equipment under the driving test, and there was no disturbance on the Ip_2 current output and NOx concentration output with an oxygen change of different magnitudes, as shown in Figure 21. The measurement accuracy and response speed of the sensor could meet the requirements of application on a vehicle.

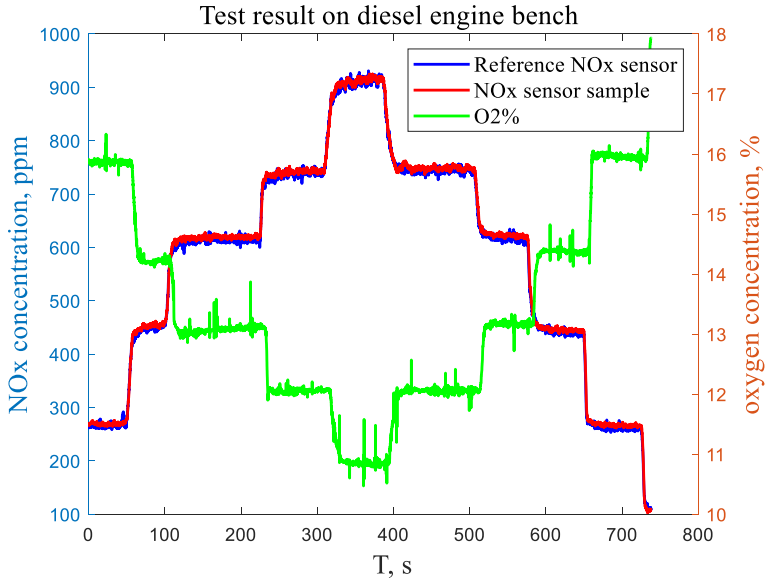

Figure 19. Test results on diesel engine bench.

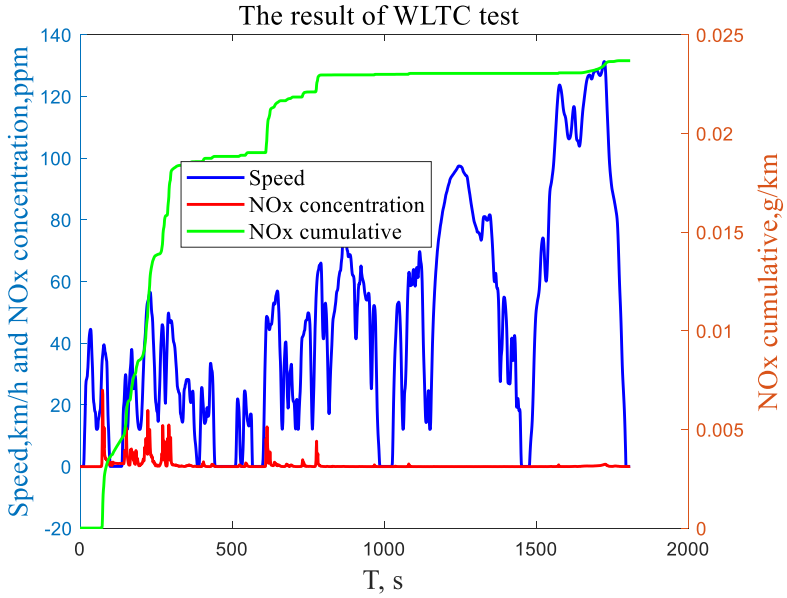

Figure 20. The results of WLTC test.

Table 5. Emission test results.

Test Name	**SDPK Test**								
Test Record Name	**WLTC Class3b SDPK Vehicle 20200430 2**								
Gas composition	CO_2	CO	THC	CH_4	NMHC	NOX	HC + NOX	NMHC + NOX	N_2O
unit	g/km	mg/km	mg/km	mg/km	mg/km	mg/km	mg/km	mg/km	mg/km
Dilute	239.60	154.7	27.7	14.9	18.7	23.7	51.4	42.3339	15.2
Bag	239.46	142.1	26.7	15.3	10.2	22.6	49.2	32.8058	14.8
China GB6b Class 2 _III limit	-	740	80	-	-	50	-	55	3

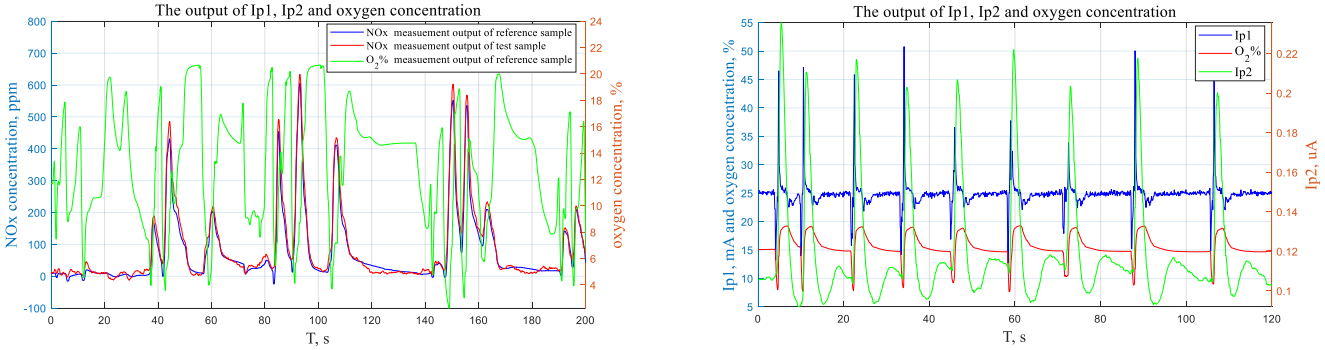

Figure 21. The dynamic output of NOx sensor under driving test.

5. Conclusions

This paper analyzes the effects of electrode activity, ceramic element structure size, and input parameters of multi-chamber closed-loop control on the accuracy and response speed characteristics of a NOx sensor in practical applications based on the application analysis and experiment. The following four conclusions can be drawn and verified in the application.

First, when the Ip_1 value is set the same, the oxygen concentration in the first chamber increases as the P− electrode activity decreases. When the P− electrode is set as a low-activity electrode, the oxygen concentration in the first chamber is high, which helps to improve the measurement accuracy of the NOx sensor in rich exhaust gas.

Second, when the Ip_1 value is set the same, the oxygen concentration in the first chamber increases as the diffusion capacity of the second diffusion channel decreases.

The value of the Ip_1 set point in the closed-loop control of Vp_0 and Ip_1 affects the response speed of the dynamic output of the Ip_2 and NOx concentration. Setting Ip_1 too small results in a low oxygen concentration in the first chamber. Then, the anti-interference ability of the Vp_0 and Ip_1 closed-loop control system decreases, resulting in a reduction in the anti-interference ability and measurement accuracy of the NOx sensor. Setting Ip_1 too large increases the oxygen concentration dependence of the NOx measurement and reduces the measurement accuracy of the NOx sensor. The activity of measurement of the P− electrode and the diffusion capacity of the second diffusion channel should be considered when setting an appropriate Ip_1 value for Vp_0 and Ip_1 closed-loop control.

Third, the influence of oxygen concentration dependence needs to be fully considered. A suitable calibration algorithm needs to be adopted to correct the measurement error caused by oxygen concentration dependence when the NOx sensor is applied on a vehicle.

Fourth, the study of the application characteristics of NOx sensors is helpful to the design of high-precision NOx sensors, which is a critical requirement in an exhaust aftertreatment system and is expected to contribute to emission reduction and global environmental protection.

Author Contributions: Conceptualization, X.L.; Data curation, J.W. and Z.W.; Formal analysis, X.L. and Z.W.; Investigation, J.W.; Methodology, J.W.; Project administration, J.F.; Resources, J.F.; Software, W.L.; Validation, J.W.; Visualization, W.L. and J.P.; Writing—original draft, J.W.; Writing—review & editing, X.L. and Z.W. All authors have read and agreed to the published version of the manuscript.

Funding: This work was funded by the National Natural Science Foundation of China (grant numbers: U2066202, 61873323) and the Shenzhen Science and Technology Innovation Committee (grant number: JCYJ20210324115606017).

Institutional Review Board Statement: Not applicable.

Informed Consent Statement: Not applicable.

Data Availability Statement: The measurement data presented in this study is available on request from the corresponding author.

Acknowledgments: We are grateful for the helpful discussions with our colleagues at Changzhou Lambda Electronics Co., Ltd.: Wenchao Feng and Xiyong Wu.

Conflicts of Interest: The authors declare no conflict of interest.

References

1. Cheng, H.; Jing, S.; Xu, Y.; Deng, Z.; Li, J.; Li, X. Control-oriented modeling analysis and optimization of planar solid oxide fuel cell system. *Int. J. Hydrog. Energy* **2016**, *41*, 22285–22304. [CrossRef]
2. Zhang, L.; Jiang, J.; Cheng, H.; Deng, Z.; Li, X. Control strategy for power management, efficiency-optimization and operating-safety of a 5-kW solid oxide fuel cell system. *Electrochim. Acta* **2015**, *177*, 237–249. [CrossRef]
3. Liu, Y.; Parisi, J.; Sun, X.; Lei, Y. Solid-state gas sensors for high temperature applications—A review. *J. Mater. Chem. A* **2014**, *2*, 9919–9943. [CrossRef]
4. Cao, H.; Deng, Z.; Li, X.; Yang, J.; Qin, Y. Dynamic modeling of electrical characteristics of solid oxide fuel cells using fractional derivatives. *Int. J. Hydrog. Energy* **2010**, *35*, 1749–1758. [CrossRef]
5. Riegel, J. Exhaust gas sensors for automotive emission control. *Solid State Ionics* **2002**, *152–153*, 783–800. [CrossRef]
6. Tao, L.; Wang, X.; Lin, L.; Yu, J. Electrochemical NOx gas sensors based on stabilized zirconia. *J. Electrochem. Soc.* **2017**, *164*, B610–B619.
7. Janardhanan, V.M.; Deutschmann, O. Modeling of Solid-Oxide Fuel Cells. *Z. Für Phys. Chem.* **2007**, *221*, 443–478. [CrossRef]
8. Praveena, V.; Martin, M.L.J. A review on various after treatment techniques to reduce NOx emissions in a CI engine. *J. Energy Inst.* **2018**, *91*, 704–720. [CrossRef]
9. Geng, P.; Tan, Q.; Zhang, C.; Wei, L.; He, X.; Cao, E.; Jiang, K. Experimental investigation on NOx and green house gas emissions from a marine auxiliary diesel engine using ultralow sulfur light fuel. *Sci. Total Environ.* **2016**, *572*, 467–475. [CrossRef]
10. Guan, B.; Zhan, R.; Lin, H.; Huang, Z. Review of state of the art technologies of selective catalytic reduction of NOx from diesel engine exhaust. *Appl. Therm. Eng.* **2014**, *66*, 395–414. [CrossRef]
11. Todo, Y.; Ichikawa, H.; Yotou, H.; Aoki, K.; Kawai, M. *Development of High Accuracy and Quick Light-off NOx Sensor*; WCX World Congress Experience: Detroit, MI, USA, 10–12 April 2018.
12. Sasaki, H.; Scholl, D.; Parsons, M.; Inagaki, H.; Shiotani, K.; Visser, J.; Zawacki, G.; Kawai, T.; Teramoto, S.; Kubinski, D. Development of an Al_2O_3/ZrO_2-Composite High-Accuracy NOx Sensor. In Proceedings of the SAE 2010 World Congress & Exhibition, Detroit, MI, USA, 13–15 April 2010. [CrossRef]
13. Sekiya, T.; Saito, N.; Kagenyama, S. Gas Sensor. U.S. Patent 9804118B2, 31 October 2017.
14. Cao, Y.; Li, Y.; Yu, Y.; Jiang, J.; Li, X. Numerical analysis and design for NOx sensor pump units decoupling control. In Proceedings of the 2019 Chinese Automation Congress (CAC), Hangzhou, China, 22–24 November 2019; pp. 5815–5820. [CrossRef]
15. Schmidt-Zhang, P.; Zhang, W.; Gerlach, F.; Ahlborn, K.; Guth, U. Electrochemical investigations on multi-metallic electrodes for amperometric NO gas sensors. *Sens. Actuators B Chem.* **2005**, *108*, 797–802. [CrossRef]
16. Walsh, K.J.; Fedkiw, P.S. Nitric oxide reduction using iridium electrodes on yttria-stabilized zirconia. *Solid State Ionics* **1997**, *104*, 97–108. [CrossRef]
17. Do, J.-S.; Chang, W.-B. Amperometric nitrogen dioxide gas sensor: Preparation of PAn/Au/SPE and sensing behaviour. *Sens. Actuators B Chem.* **2001**, *72*, 101–107. [CrossRef]
18. Dutta, A.; Ishihara, T. Amperometric NOX sensor based on oxygen pumping current by using LaGaO3-based solid electrolyte for monitoring exhaust gas. *Sens. Actuators B Chem.* **2005**, *108*, 309–313. [CrossRef]
19. Nakamura, T.; Sakamoto, Y.; Saji, K.; Sakata, J. NOx decomposition mechanism on the electrodes of a zirconia-based amperometric NOx sensor. *Sens. Actuators B Chem.* **2003**, *93*, 214–220. [CrossRef]
20. de Lucas-Consuegra, A.; Caravaca, Á.; Dorado, F.; Valverde, J.L. Pt/K–βAl_2O_3 solid electrolyte cell as a "smart electrochemical catalyst" for the effective removal of NOx under wet reaction conditions. *Catal. Today* **2009**, *146*, 330–335. [CrossRef]
21. Gao, J.; Hua, Z.; Xu, S.; Wan, H.; Zhi, Z.; Chen, X.; Fan, S. Amperometric gas sensors based on screen printed electrodes with porous ceramic substrates. *Sens. Actuators B Chem.* **2021**, *342*, 130045. [CrossRef]
22. Yang, J.-C.; Dutta, P.K. High temperature amperometric total NOx sensors with platinum-loaded zeolite Y electrodes. *Sens. Actuators B Chem.* **2007**, *123*, 929–936. [CrossRef]
23. Kaneko, H. Reduction of pulse-injected nitric monoxide using a zirconia oxygen pump-gauge. *Solid State Ion.* **2000**, *136–137*, 607–612. [CrossRef]
24. Bashir, M.; Patri, S.R.; Krishnaprasad, K. A low power, high accuracy amperometric potentiostat for NOx gas sensors. In Proceedings of the International Conference on Next Generation Intelligent Systems (ICNGIS), Kottayam, India, 1–3 September 2016; pp. 1–4. [CrossRef]
25. Aliramezani, M.; Koch, C.R.; Patrick, R. Phenomenological model of a solid electrolyte NOx and O_2 sensor using temperature perturbation for on-board diagnostics. *Solid State Ion.* **2018**, *321*, 62–68. [CrossRef]
26. Aliramezani, M.; Koch, C.R.; Hayes, R.E.; Patrick, R. Amperometric solid electrolyte NOx sensors—The effect of temperature and diffusion mechanisms. *Solid State Ionics* **2017**, *313*, 7–13. [CrossRef]
27. Auckenthaler, T.S.; Onder, C.H.; Geering, H.P. Modelling of a Solid-Electrolyte Oxygen Sensor. *SAE Trans.* **2002**, *111*, 2162–2171. [CrossRef]

28. Chen, Z.; Wang, J.; Wang, Y. Strategies for the performance enhancement of graphene-based gas sensors: A review. *Talanta* **2021**, *235*, 122745. [CrossRef] [PubMed]
29. Wang, Z.; Deng, Z.-H.; Zhu, R.-J.; Zhou, Y.-H.; Li, X. Modeling and analysis of pumping cell of NOx sensor—Part I: Main oxygen pumping cell. *Sens. Actuators B Chem.* **2022**, *359*, 131622. [CrossRef]
30. Mitterdorfer, A.; Gauckler, L. Reaction kinetics of the Pt, O_2(g) | c-ZrO_2 system: Precursor-mediated adsorption. *Solid State Ionics* **1999**, *120*, 211–225. [CrossRef]
31. Velle, O.; Norby, T.; Kofstad, P. The electrode system O2Pt||ZrO2: 8Y2O3 investigated by impedence spectroscopy. *Solid State Ionics* **1991**, *47*, 161–167. [CrossRef]
32. Okamoto, H.; Kawamura, G.; Kudo, T. Study of oxygen adsorption on platinum through observation of exchange current in a solid electrolyte concentration cell. *Electrochim. Acta* **1983**, *28*, 379–382. [CrossRef]
33. Brailsford, A.; Yussouff, M.; Logothetis, E. Theory of gas sensors: Response of an electrochemical sensor to multi-component gas mixtures. *Sens. Actuators B Chem.* **1996**, *34*, 407–411. [CrossRef]
34. Kato, N.; Kurachi, H.; Hamada, Y. Thick Film ZrO2 NOx Sensor for the Measurement of Low NOx Concentration. In Proceedings of the SAE International Congress & Exposition, Detroit, MI, USA, 23–27 February 1998; Volume 107, pp. 312–320. [CrossRef]
35. Sekiya, T.; Saito, N.; Kageyama, S. Gas Sensor. U.S. Patent 0276659A1, 1 October 2015.
36. Fujita, H.; Kasugai; Shindo, H. Sensor Element and Gas Sensor. U.S. Patent 9804139B2, 31 October 2017.